Hindawi
Shock and Vibration
Volume 2018, Article ID 6292595, 12 pages
https://doi.org/10.1155/2018/6292595

Research Article

Decoupling Optimization Design of Under-Chassis Equipment Suspension System in High-Speed Trains

Zhanghui Xia, Dao Gong, Jinsong Zhou, Wenjing Sun, and Yu Sun

Institute of Rail Transit, Tongji University, Shanghai, China

Correspondence should be addressed to Dao Gong; gongdao@tongji.edu.cn

Received 3 July 2018; Accepted 4 September 2018; Published 3 October 2018

Academic Editor: Chengzhi Shi

The vibrations of high-speed trains may strongly affect the safety and ride comfort of passengers, which issue requires the damping optimization of under-chassis equipment (UCE). In this study, the natural frequency of UCE is determined via the dynamic vibration absorber theory. The performed investigation of UCE-car body system vibration behavior revealed that an eccentricity of UCE results in the coupling vibration in six degrees of freedom, which leads to significant changes in its vibration mode and frequency. Thus, the natural frequency of UCE deviates from the initially determined value, which implies that the vibration damping effect is weakened. In this study, two decoupling optimization design methods, namely, forward and inverse decoupling methods, are proposed to solve this problem. The analysis of results obtained proves the feasibility of the proposed methods, which yield favorable decoupling degrees for the UCE vibration modes and minimize the offset of the vibration mode frequency from the initial natural one. These methods are considered quite instrumental in the improvement of vibration damping effect for high-speed trains.

1. Introduction

Nowadays, the power decentralization technology has been widely applied in high-speed electric multiple unit (EMU) trains. As compared to centralized power trains, the decentralized ones can take full advantage of the wheel-track adhesive force. As a result, the decentralized power trains effectively reduce the dynamic wheel-track interaction force and noise, as well as exhibit flexible marshaling and high-power traction of high-speed trains. Power decentralized high-speed EMU trains are configured with more elements of under-chassis equipment (UCE), such as traction converters and auxiliary current transformers. Since some UCE elements have significant volume and mass, any errors in the design of their damping capacity may imply severe adverse effects on the local and overall vibration performance of the speed-train car body.

To reduce the vibration amplitude, suspension systems of UCE are usually attached using rubber components. Gong et al. [1] studied the influence of the UCE suspension system parameters on the first-order vertical bending frequency of a high-speed EMU train car body. Moreover, the parameters of the UCE suspension system were designed based on the mode matching principle. Zhou et al. [2, 3] analyzed the inhibiting effect of adopting a dynamic vibration absorber (DVA) on the car body elastic oscillation by elaborating a vertical rigid-flexible dynamical model of railway vehicles containing UCE. At present, DVAs are widely used as passive damping systems [4–6].

However, in previous studies, UCE was mostly reduced to a point with a single degree-of-freedom (DOF), although, in fact, it is a three-dimensional body with 6 DOF. Moreover, due to available barycenter offset, local mass inappropriate distribution, and unreasonable suspension system design of UCE, the coupling of vibrations in six DOFs is likely to occur, which deteriorates the damping effect on the car body vibration. The decoupling degree is one of the major indices used to evaluate the quality of suspension systems. The higher the decoupling degree, the better the vibration independence in each direction. In other words, better vibration independence in each direction (achieved by such decoupling) is beneficial for optimizing the UCE vibration frequency in each direction [7, 8]. Therefore, in this paper, the UCE natural frequency optimization was designed firstly. Next, the influence of UCE coupling vibration on the vehicle vibration performance and related mechanism were studied. Finally,

two decoupling optimization design methods were proposed. Accordingly, the dynamic performances of car body were also analyzed. The research results obtained are considered instrumental in the UCE design, which would ensure the reduction of vibrations in high-speed EMU trains.

2. Rigid-Flexible Coupling Dynamic Model

In more in-depth investigations of vehicle systems, the car body should be considered as a flexible system with dynamic deformation, in order to more accurately reflect the complex dynamic features of the car body [9, 10]. As compared to previously used simplified rigid systems, flexible ones can reveal the influence of self-deformation on the vehicle vibration, which makes the simulation test of the virtual prototype closer to actual conditions. In the modeling process, to construct a rigid-flexible coupling dynamics model of a vehicle system with the account of the car body elasticity, the Hypermesh software, which allows one to elaborate the refined finite element model of high-speed EMU train car body, was used. Next, a vehicle rigid-flexible coupling system dynamics model containing an elastic car body was developed using the Simpack software.

Figure 1 shows the elastic modal calculation for the first five orders of vibration modes, in which (a) is diamond-shaped deformation mode at 9.70 Hz; (b) first-order vertical bending mode at 11.52 Hz; (c) breathing mode at 14.35 Hz; (d) first-order torsional mode at12.42 Hz; and (e) first-order lateral bending mode at 14.16 Hz. The car body finite element model was reduced based on the reduction theory [11]. Table 1 lists the modal frequency calculation results of low-order elastic modal vibration modes of the car body before and after the above reduction. Insofar as the modal frequencies before and after the reduction differ by no more than 3%, such reduction is considered acceptable.

The reduction data file containing car body structure and modal information was imported into the vehicle dynamics model. Only five orders of elastic modes listed in Table 1 were considered in the car body elasticity according to its contribution to the vibration energy [12]. The developed vehicle rigid-flexible coupling system dynamics model containing an elastic car body is illustrated by Figure 2. The model consists of an elastic car body, two bogies, eight axle boxes, four wheelsets, and one UCE (four suspended rubber components). The bogies, axle boxes, wheelsets, and UCE are treated as rigid bodies. In the model, the following nonlinear factors were considered: the wheel-track contact nonlinear geometrical feature, the nonlinear creep force and moment, the stiffness increasing pattern of the two-stage transverse elastic behavior, and the nonlinear response of the hydraulic shock absorber.

3. Determination of UCE Natural Frequency

Elastic suspension systems are usually adopted during the vibration reduction design of UCE to reduce the adverse effect on the car body vibration caused by UCE. By the design strategies, the vibration reduction design can be roughly classified into active vibration reduction, vibration damping, and vibration isolation [13, 14]. In this paper, a design method based on the DVA theory is utilized to derive the natural frequency of UCE. The loading device is used to produce the force, which is applied to the main system by DVA counteracting with the exciting external force that is applied to the main system. Thus, it inhibits the vibration of the main system. By setting the car body as the main system while setting UCE as DVA, and by setting the ratio of the vertical vibration natural frequency of UCE to the car body self-vibration frequency, which meets the optimal homology condition, the following equation can be obtained via the fix-point theory [15]:

$$\gamma_{\text{opt}} = \frac{f_{\text{eo}}}{f_{\text{co}}} = \frac{1}{\sqrt{1+\mu}}, \tag{1}$$

where f_{eo} is the vertical vibration natural frequency of UCE, f_{co} is the car body self-vibration frequency, and μ is the mass ratio of UCE to the car body. According to the contribution of the car body elastic modal vibration to the car body vibration [3], the car body vertical first-order bending modal frequency is selected as the car body self-vibration frequency.

In this paper, the car body mass is 32.65 t, the equipment mass is 6.4 t, and the car body vertical first-order bending modal frequency is 11.60 Hz. It is implied that the vertical optimal natural frequency of UCE is 10.60 Hz, which is close to the car body vertical first-order bending modal frequency of 11.60 Hz.

According to the natural frequency of UCE vertical vibration, the three-directional stiffness of rubber components can be obtained by adopting the traditional rubber component stiffness design method. In the conventional design method, the vertical stiffness of rubber component k_{zo} can be calculated using the following equation:

$$k_{\text{zo}} = \frac{m \cdot (2\pi f_{\text{eo}})^2}{n}, \tag{2}$$

where m is UCE mass, f_{eo} is UCE vertical designed frequency, and n is the number of UCE suspended points.

According to the manifestation features, the transverse and longitudinal stiffness of the rubber component is usually related to the vertical stiffness value. When the rubber component is under tension, the vertical (compression direction) stiffness is 2–3 times higher than the transverse one. The longitudinal stiffness is usually large (1–3 times higher than the vertical one) because the stop block exists in the equipment's longitudinal direction. In this section, the transverse-vertical stiffness ratio is 1/3, and the longitudinal-vertical one is equal to 2, according to Equations. (3) and (4), respectively:

$$k_{\text{yo}} = \frac{k_{\text{zo}}}{3}, \tag{3}$$

$$k_{\text{xo}} = 2k_{\text{zo}}. \tag{4}$$

Based on the vehicle rigid-flexible coupling dynamics model depicted in Figure 2, the effect of UCE natural frequency on the car body vibration is investigated with the UCE vibration reduction design. The low-excitation high-speed range is adopted in track unevenness [16]. The vehicle running speed values under study are 200 and 300 km/h. The UCE vertical natural frequency is between 6 and 16 Hz.

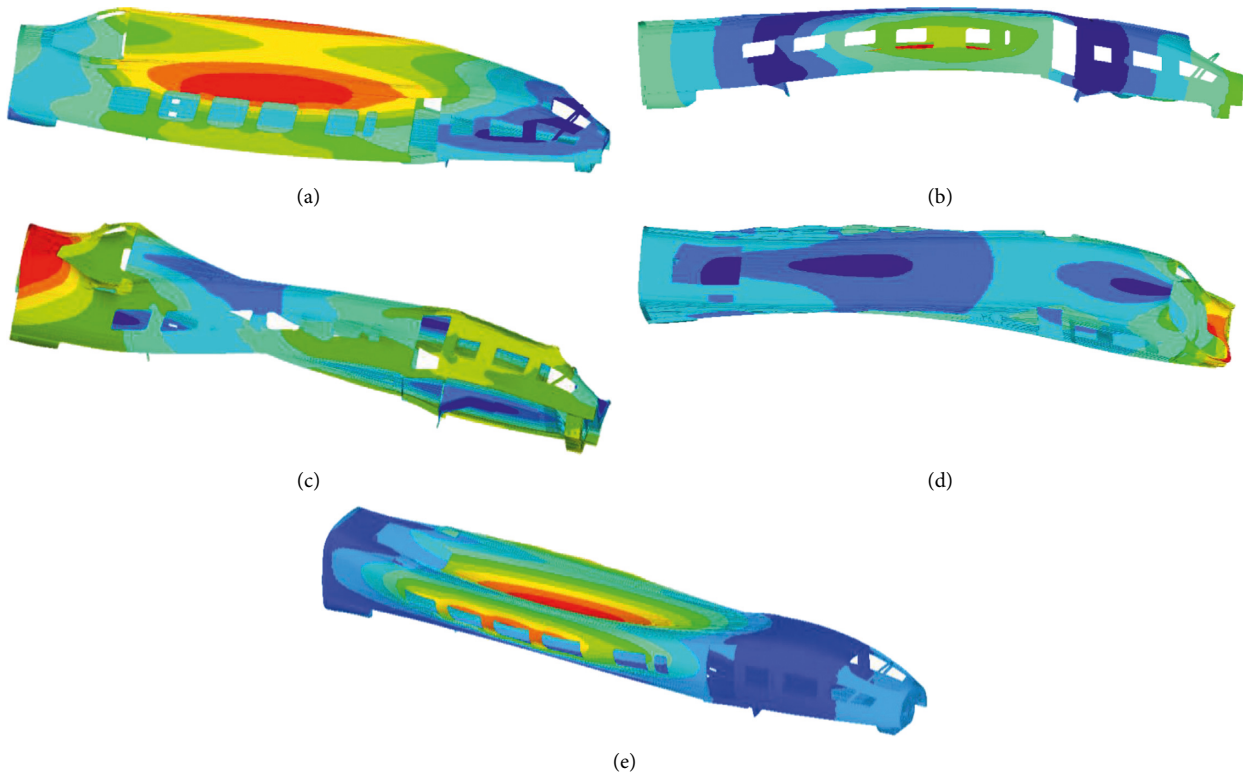

Figure 1: The eigen frequency results for the first five orders of the car body vibrations.

Table 1: Car body elastic modal frequencies (Hz).

Vibration mode	Before reduction	After reduction	Deviation (%)
First-order diamond-shaped deformation	9.70	9.66	0.41
Vertical first-order bending	11.52	11.60	0.69
First-order torsion	12.42	12.44	0.16
First-order lateral bending	14.16	14.32	1.13
First-order breathing	14.35	14.55	1.39

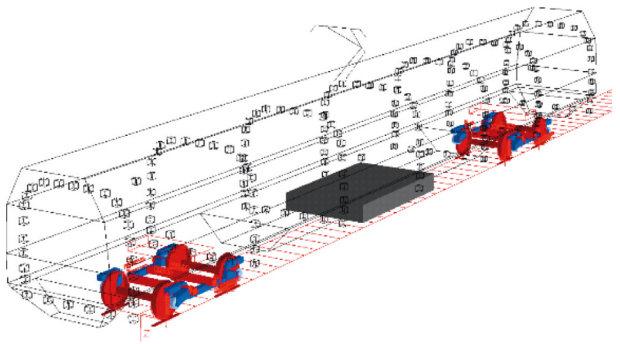

Figure 2: Vehicle rigid-flexible coupling dynamics model.

The three-directional stiffness of the rubber component is obtained via Equations (2)–(4). The damping ratio of the rubber component is 0.06. Figures 3–5 depict the following calculation results: vertical acceleration of UCE mass center, the vertical acceleration effective value of the car body center

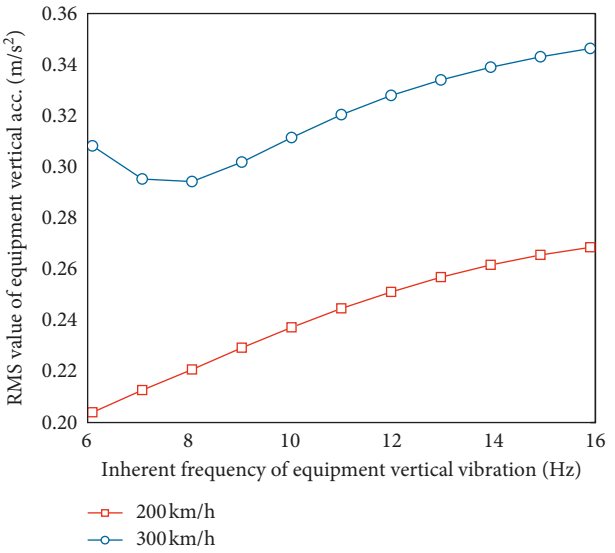

Figure 3: RMS value of UCE vertical vibration acceleration.

(RMS value), and the vertical Sperling index of the car body center [17], respectively. As shown in Figure 3, the RMS value of UCE vertical vibration acceleration increases with the improvement of UCE vertical natural frequency when the vehicle running speed is 200 km/h. When the latter is 300 km/h, the RMS value of UCE vertical vibration acceleration firstly drops and then increases, accompanied by an increase in UCE vertical natural frequency. According to Figures 4 and 5, both RMS value of the vertical acceleration

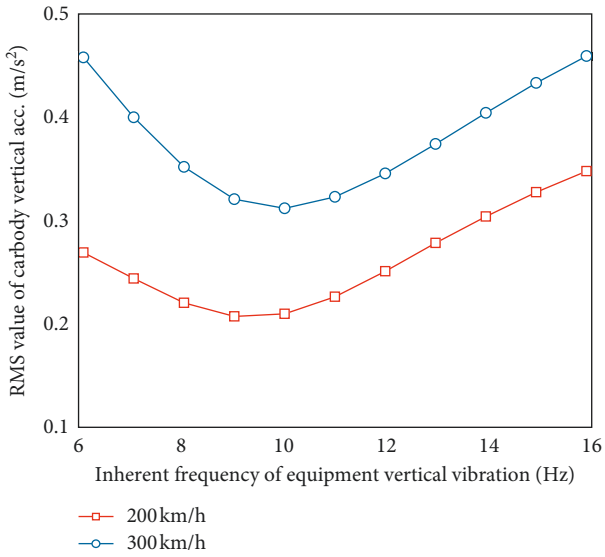

Figure 4: RMS value of the car body vertical vibration acceleration.

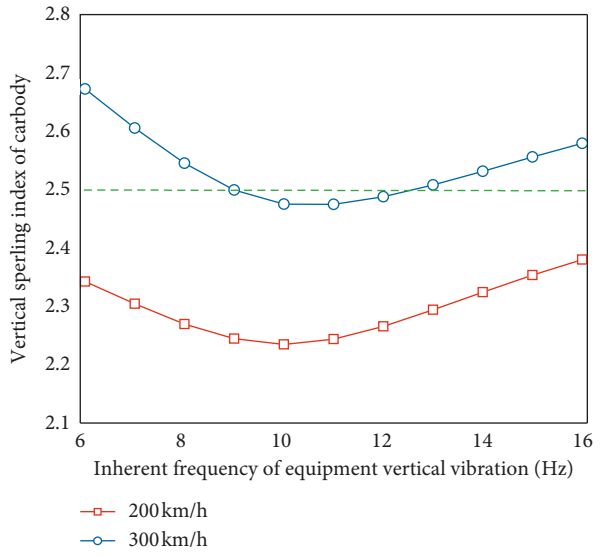

Figure 5: Vertical Sperling index of the car body.

vibration and vertical Sperling index of the car body center exhibit the same "drop and rise" tendency. Also, with the improvement of equipment vertical vibration natural frequency, both reach their minimum values between 10 and 11 Hz. By comprehensively considering the design result based on the DVA theory and car body vibration results, UCE vertical vibration natural frequency vibration is determined as 10.5 Hz.

4. Influence of UCE Coupling Vibration on the DVA Effect

In the analyses mentioned above, the coupling vibration between six DOFs of UCE has not been taken into consideration. Hence, this section considers one of the operation conditions induced by UCE coupling vibration (the influence of gravity center offset) to investigate the impact of the coupling vibration on the DVA effect. Some UCE components have large volume and mass values. Moreover, some UCE components attached to the under-chassis side beam share the same space with as other equipment. Thus, eccentricity conditions often exist in UCE, i.e., the gravity center does not always coincide with its geometrical center. In practice, the eccentricity of UCE can be subdivided into transverse and longitudinal eccentricity cases (Figure 6). This section is focused on the influence of UCE eccentricity on the vehicle ride quality. During analysis, the natural frequency of UCE vertical vibration is designed as 10.5 Hz. Only the transverse and longitudinal eccentricities at one side of UCE symmetry axis are considered, insofar as the car body and UCE are axisymmetric, and UCE is suspended at the car body center.

Figure 7 shows the calculation results of the vehicle vertical Sperling index when UCE transverse eccentricity is between 0 and 0.8 m. This demonstrates that the transverse eccentricity of UCE has a significant influence on the vehicle vertical ride quality. When the vehicle running speed reaches 300 km/h and the transverse eccentric distance exceeds 0.6 m, the car body vertical Sperling index is higher than 2.5. That is, the ride quality level is deteriorated from the standard of excellence to the level of "good."

Figure 8 shows the calculation results of vehicle vertical Sperling index when UCE longitudinal eccentric distance is between 0 and 1.0 m. As shown in Figure 8 (similar to the influence regularity of transverse eccentricity), the longitudinal eccentricity of UCE has a significant influence on the vehicle vertical ride quality. When the vehicle running speed reaches 300 km/h, and the eccentric longitudinal distance is greater than 0.5 m, the vehicle vertical Sperling index is higher than 2.5, and the ride quality level decreases to "good."

The above analysis indicates that, although UCE adopts the rubber stiffness value under the measured natural frequency, there is a significant influence of UCE transverse and longitudinal eccentricity on the vehicle vertical ride quality. Hence, if the coupling vibration of UCE is not considered in detail during the vibration reduction design, the damping effect is very likely to deviate from the design expectation, which leads to a severe deterioration of the damping effect. Hence, the influence mechanism of UCE coupling vibration on the dynamic vehicle performance should be carefully studied.

5. Mechanism of Coupling Vibration and DVA Effect Interaction

5.1. Free Vibration Equation of UCE. UCE is treated as a rigid spatial body with six DOF, while rubber components are regarded as springs with three-directional stiffness. The coordinate system of UCE is defined as follows: the origin of the coordinates is the barycenter position of UCE, the vehicle riding direction is positive x-direction, the right side of the vehicle riding direction is a positive y-direction, and the downward direction is a positive z-direction. The roll (r_x), pitch (r_y), and yaw (r_z) directions are determined according to the right-hand rule. Figure 9 schematically presents the UCE coordinate system.

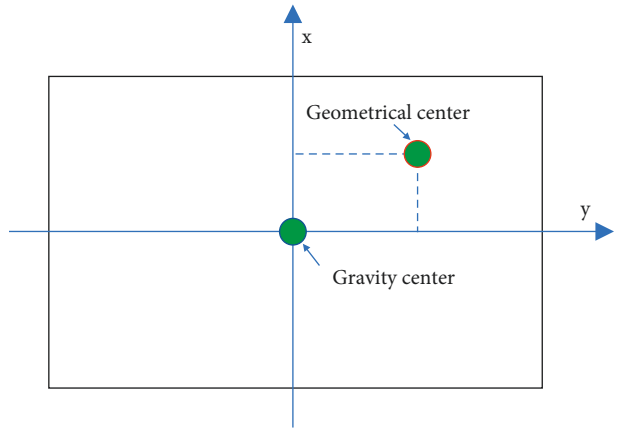

Figure 6: The eccentricity of UCE.

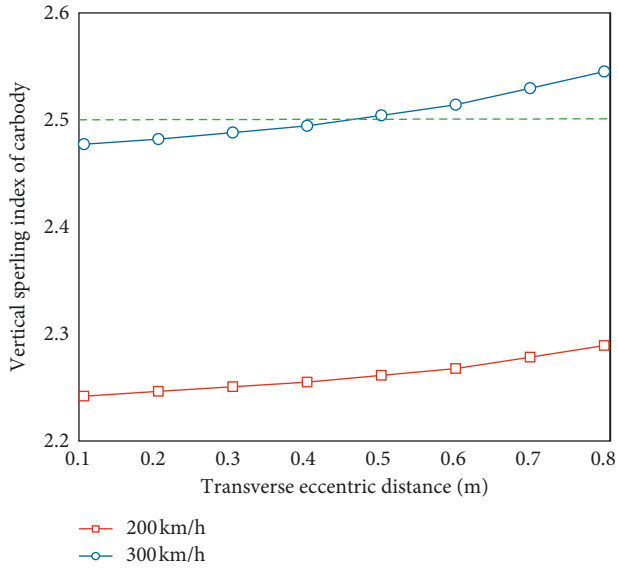

Figure 7: Influence of UCE transverse eccentricity on the vertical Sperling index.

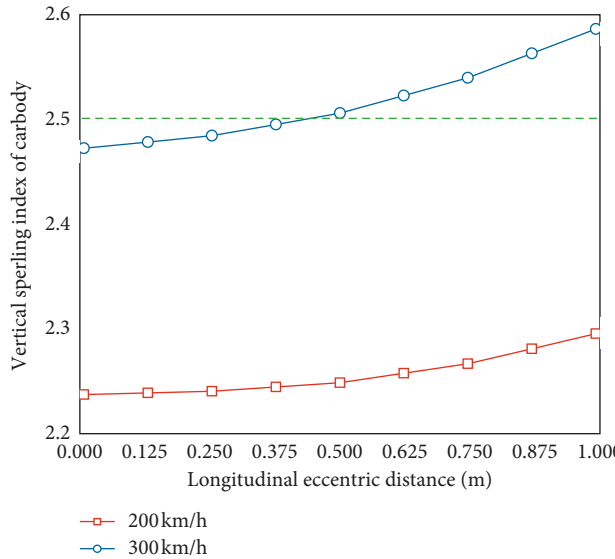

Figure 8: Influence of UCE longitudinal eccentricity on the vertical Sperling index.

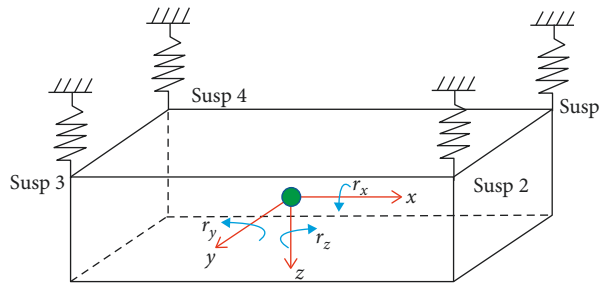

Figure 9: Schematic representation of the UCE coordinate system.

The coordinates of the ith ($i = 1, 2, 3, 4$) rubber component are (a_i, b_i, c_i), while their three-directional stiffness is (k_{xi}, k_{yi}, k_{zi}). When UCE vibrates, the elastic force and moment generated by the ith rubber component are as follows:

$$\begin{cases} F_{xi} = k_{xi}\left(x + c_i r_y - b_i r_z\right), \\ F_{yi} = k_{yi}\left(y + a_i r_z - c_i r_x\right), \\ F_{zi} = k_{zi}\left(z + b_i r_x - a_i r_y\right), \\ M_{xi} = F_{zi} b_i - F_{yi} c_i, \\ M_{yi} = F_{xi} c_i - F_{zi} a_i, \\ M_{zi} = F_{yi} a_i - F_{xi} b_i, \end{cases} \quad i = 1, 2, 3, 4. \tag{5}$$

In the above equation, $\mathbf{T} = [x, y, z, r_x, r_y, r_z]^{\mathrm{T}}$ is the rigid body displacement along six DOF of UCE. The overall elastic force and moment produced by four rubber components are as follows:

$$\mathbf{O}_{\mathrm{FM}} = \sum_{i=1}^{4} \left[F_{xi}, F_{yi}, F_{zi}, M_{xi}, M_{yi}, M_{zi}\right]^{\mathrm{T}}. \tag{6}$$

Without considering the external excitation, the dynamics equation for UCE with six DOF of the can be reduced to

$$\mathbf{M}\ddot{\mathbf{T}} + \mathbf{O}_{\mathrm{FM}} = 0, \tag{7}$$

where m is UCE mass and I_{xx}, I_{yy}, and I_{zz} are rotational inertia of UCE along the respective axes.

By expanding and rearranging Equation (7), we can get the following:

$$\begin{cases} m\ddot{x} + \left(\sum_{i=1}^{4} k_{xi}\right)x + \left(\sum_{i=1}^{4} k_{xi}c_i\right)r_y - \left(\sum_{i=1}^{4} k_{xi}b_i\right)r_z = 0, \\ m\ddot{y} + \left(\sum_{i=1}^{4} k_{yi}\right)y - \left(\sum_{i=1}^{4} k_{yi}c_i\right)r_x + \left(\sum_{i=1}^{4} k_{yi}a_i\right)r_z = 0, \\ m\ddot{z} + \left(\sum_{i=1}^{4} k_{zi}\right)x + \left(\sum_{i=1}^{4} k_{zi}b_i\right)r_x - \left(\sum_{i=1}^{4} k_{zi}a_i\right)r_y = 0, \\ I_{xx}\ddot{r}_x - \left(\sum_{i=1}^{4} k_{yi}c_i\right)y + \left(\sum_{i=1}^{4} k_{zi}b_i\right)z + \left[\left(\sum_{i=1}^{4} k_{zi}b_i^2\right) + \left(\sum_{i=1}^{4} k_{yi}c_i^2\right)\right]r_x - \left(\sum_{i=1}^{4} k_{zi}a_i b_i\right)r_y - \left(\sum_{i=1}^{4} k_{yi}a_i c_i\right)r_z = 0, \\ I_{yy}\ddot{r}_y + \left(\sum_{i=1}^{4} k_{xi}c_i\right)x - \left(\sum_{i=1}^{4} k_{zi}a_i\right)z - \left[\left(\sum_{i=1}^{4} k_{zi}a_i b_i\right)r_x + \left(\sum_{i=1}^{4} k_{zi}c_i^2\right) + \left(\sum_{i=1}^{4} k_{zi}a_i^2\right)\right]r_y - \left(\sum_{i=1}^{4} k_{xi}b_i c_i\right)r_z = 0, \\ I_{zz}\ddot{r}_z - \left(\sum_{i=1}^{4} k_{xi}b_i\right)x + \left(\sum_{i=1}^{4} k_{yi}a_i\right)y - \left(\sum_{i=1}^{4} k_{yi}a_i c_i\right)r_x - \left(\sum_{i=1}^{4} k_{zi}b_i c_i\right)r_y + \left[\left(\sum_{i=1}^{4} k_{yi}a_i^2\right) + \left(\sum_{i=1}^{4} k_{xi}b_i^2\right)\right]r_z = 0. \end{cases} \tag{8}$$

According to Equation (8), the six-order rigid body vibration mode vectors and modal frequencies of UCE are solved as follows:

$$\mathbf{K}\mathbf{T}_j = \lambda_j \mathbf{M}\mathbf{T}_j, \quad j = 1, 2, 3, 4, 5, 6, \tag{9}$$

where $\mathbf{T}_j = [x, y, z, r_x, r_y, r_z]_j^{\mathrm{T}}$ is the six-freedom-degree displacement of each modal vector; $\lambda_j = (2\pi f_j)^2$ is the modal characteristic value of each order; f_j is the modal frequency of each order; and $\mathbf{K}$ is the stiffness matrix of UCE, which is expressed as follows:

$$\mathbf{K} = \begin{bmatrix} K_{11} & 0 & 0 & 0 & K_{15} & K_{16} \\ 0 & K_{22} & 0 & K_{24} & 0 & K_{26} \\ 0 & 0 & K_{33} & K_{34} & K_{35} & 0 \\ 0 & K_{42} & K_{43} & K_{44} & K_{45} & K_{46} \\ K_{51} & 0 & K_{53} & K_{54} & K_{55} & K_{56} \\ K_{61} & K_{62} & 0 & K_{64} & K_{65} & K_{66} \end{bmatrix}, \quad (10)$$

where the matrix diagonal elements K_{11}, K_{22}, K_{33}, K_{44}, K_{55}, and K_{66} are linear and angular stiffness factors, which are as follows:

$$\begin{cases} K_{11} = \sum k_{xi}, \\ K_{22} = \sum k_{yi}, \\ K_{33} = \sum k_{zi}, \\ K_{44} = \sum \left(k_{zi} b_i^2 + k_{yi} c_i^2\right), \\ K_{55} = \sum \left(k_{xi} c_i^2 + k_{zi} a_i^2\right), \\ K_{66} = \sum \left(k_{yi} a_i^2 + k_{xi} b_i^2\right), \end{cases} \quad (11)$$

K_{15}, K_{16}, K_{24}, K_{26}, K_{34}, and K_{35} are coupling stiffness factors of linear and angular vibrations, which can be expressed as follows:

$$\begin{cases} K_{15} = K_{51} = \sum k_{xi} c_i, \\ K_{16} = K_{61} = -\sum k_{xi} b_i, \\ K_{26} = K_{62} = \sum k_{yi} a_i, \\ K_{24} = K_{42} = -\sum k_{yi} c_i \\ K_{34} = K_{43} = \sum k_{zi} b_i, \\ K_{35} = K_{53} = -\sum k_{zi} a_i, \end{cases} \quad (12)$$

K_{45}, K_{46}, and K_{56} are coupling stiffness factors of yaw and pitch vibrations, which are represented as follows:

$$\begin{cases} K_{45} = K_{54} = -\sum k_{zi} a_i b_i, \\ K_{46} = K_{64} = -\sum k_{yi} a_i c_i, \\ K_{56} = K_{65} = -\sum k_{xi} b_i c_i. \end{cases} \quad (13)$$

5.2. Energy Decoupling Degree. The jth order vibration energy distribution matrix of UCE is defined as follows [18]:

$$\mathbf{EM}(p,k) = \frac{f_j^2 \mathbf{M}(p,k) \mathbf{T}_j^p \mathbf{T}_j^k}{2}, \quad (14)$$

where $\mathbf{M}(p,k)$ is the element in the pth line and kth row of the inertia matrix; and $\mathbf{T}_j^p$ and $\mathbf{T}_j^k$ are the pth and kth elements in the jth order vibration mode vector.

The energy distribution share of the pth element by the jth order vibration mode in the total energy of the vibration mode $\mathbf{T}_j$ is as follows:

$$\mathbf{EP}(k, j) = \frac{\sum_{p=1}^{6} \mathbf{EM}(p,k)}{\sum_{k=1}^{6} \sum_{p=1}^{6} \mathbf{EM}(p,k)}. \quad (15)$$

The decoupling degree of the jth order vibration mode is defined as the share of the vibration energy in the major vibration direction of this order than the total vibration mode energy. If $\mathbf{EP}(k, j) = 100\%$, the energy of the jth order vibration mode $\mathbf{T}_j$ is concentrated in the kth element, i.e., the vibration of the jth order vibration mode of UCE is completely decoupled. Hence, the matrix **EP** can be utilized to describe the dynamic features of the system.

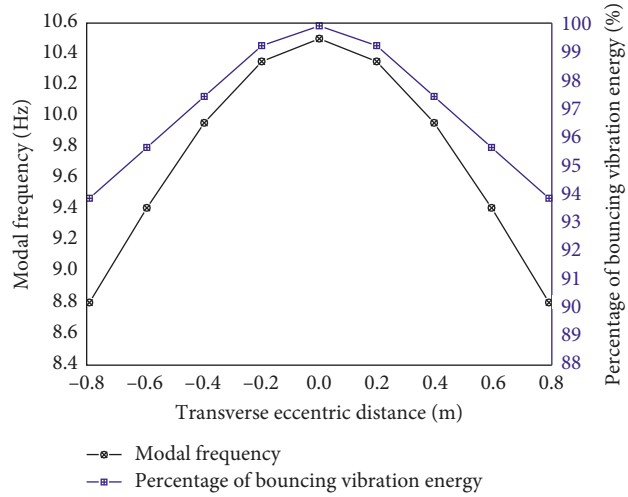

Figure 10: Influence of the transverse eccentricity on the modal frequency and energy distribution.

5.3. Study of the Influence Mechanism. The six-order rigid body modal frequency and energy distribution of UCE under transverse and longitudinal eccentric conditions are calculated to study the influence mechanism of UCE coupling vibration on the DVA effect. Figure 10 shows the vibration mode frequency of UCE when the bouncing vibration is dominant, as well as its share in the total energy of this vibration mode, in case of transverse eccentricity. As seen in Figure 10, with an increase in the absolute value of transverse eccentric distance, the vibration frequency drops, while the bouncing vibration is dominant. The bouncing vibration energy share also decreases, which indicates the increase of the coupling degree of this vibration-mode order. This is attributed to the fact that this vibration mode order is not a pure bouncing vibration mode, and that its vibration frequency is reduced. Due to the occurrence of coupling, the vertical vibration frequency of UCE deviates from the initially determined value, which leads to the deterioration of damping effect and vehicle ride quality (Figure 7).

Figure 11 depicts the vibration mode frequency of UCE with dominant bouncing vibration, in case of longitudinal eccentricity. It also shows the share of bouncing vibration energy in the total energy of this vibration mode. Similarly, with an increase in the absolute value of eccentric longitudinal distance, the share of bouncing vibration energy is reduced, while the coupling degree of the vibration mode increases. This is due to the occurrence of coupling between the bouncing vibration and vibration of other mode orders that are caused by the longitudinal eccentricity. On the contrary, the vertical vibration frequency of UCE decreases and deviates from the optimal design value. This results in the deterioration of

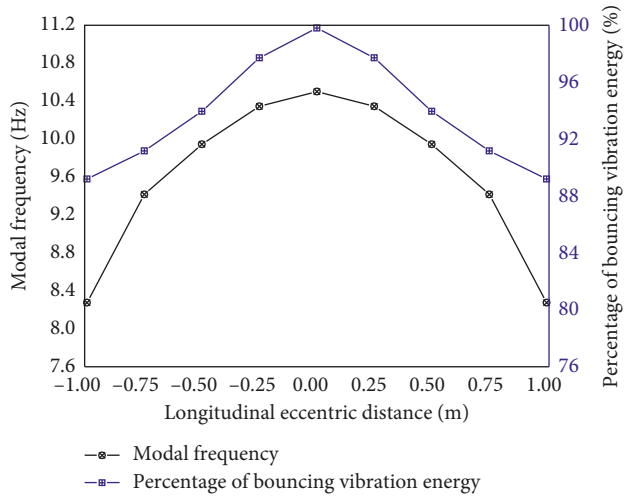

FIGURE 11: Influence of the longitudinal eccentricity on the modal frequency and energy distribution.

damping effect and vehicle ride quality (Figure 8). Based on the above findings, one may conclude that the equipment eccentricity will lead to the coupling between UCE bouncing vibration and the vibration of other vibration mode orders. Thereby, the frequency of oscillation (with dominant bouncing vibration) decreases and deviates from the initially determined natural frequency. Thus, the damping effect and vehicle ride quality are both deteriorated. Therefore, it is necessary to develop decoupling optimization methods for UCE.

6. Decoupling Optimization Methods

6.1. Forward Decoupling Method (FDM). The forward decoupling method (FDM) is based on the UCE vibration equation. By eliminating or weakening the coupling stiffness factors of linear and angular vibrations, we can obtain the analytical solution of the stiffness vector of a rubber element, for which six DOF of UCE are strictly independent at the optimal frequency. If a particular mode has only one (x-direction) displacement, the mode vector can be expressed as a unit column vector $\mathbf{T}_x = [1, 0, 0, 0, 0, 0]^{\mathrm{T}}$. If the mode frequency of this mode is equal to the optimal frequency f_{xo}, the free vibration equation of this mode takes the following form:

$$\mathbf{K}\mathbf{T}_{\mathrm{x}} = (2\pi f_{\mathrm{xo}})^2 \mathbf{M}\mathbf{T}_{\mathrm{x}}. \tag{16}$$

According to Equation (16), the first column of the stiffness matrix $\mathbf{K}$ can be obtained as follows:

$$\begin{cases} K_{11} = \sum_{i=1}^{4} k_{xi} = m(2\pi f_{\mathrm{xo}})^2, \\ K_{51} = \sum_{i=1}^{4} k_{xi} c_i = 0, \\ K_{61} = -\sum_{i=1}^{4} k_{xi} b_i = 0. \end{cases} \tag{17}$$

For the modes containing only y- and z-direction displacements, columns 2-3 of the stiffness matrix can be derived from the modal frequencies f_{yo} and f_{zo}. Similarly, columns 4–6 of the stiffness matrix can be obtained from the modal frequencies f_{rxo}, f_{ryo}, and f_{rzo}.

These equations can be written in the following matrix form:

$$\mathbf{C}\mathbf{X} = \mathbf{D}. \tag{18}$$

Here $\mathbf{C}$, $\mathbf{X}$, and $\mathbf{D}$ are as follows:

$$\mathbf{C} = \begin{bmatrix} 1 & 1 & 1 & 1 & 0 & 0 & 0 & 0 & 0 & 0 & 0 & 0 \\ c_1 & c_2 & c_3 & c_4 & 0 & 0 & 0 & 0 & 0 & 0 & 0 & 0 \\ -b_1 & -b_2 & -b_3 & -b_4 & 0 & 0 & 0 & 0 & 0 & 0 & 0 & 0 \\ 0 & 0 & 0 & 0 & 1 & 1 & 1 & 1 & 0 & 0 & 0 & 0 \\ 0 & 0 & 0 & 0 & -c_1 & -c_2 & -c_3 & -c_4 & 0 & 0 & 0 & 0 \\ 0 & 0 & 0 & 0 & a_1 & a_2 & a_3 & a_4 & 0 & 0 & 0 & 0 \\ 0 & 0 & 0 & 0 & 0 & 0 & 0 & 0 & 1 & 1 & 1 & 1 \\ 0 & 0 & 0 & 0 & 0 & 0 & 0 & 0 & b_1 & b_2 & b_3 & b_4 \\ 0 & 0 & 0 & 0 & 0 & 0 & 0 & 0 & -a_1 & -a_2 & -a_3 & -a_4 \\ 0 & 0 & 0 & 0 & c_1^2 & c_2^2 & c_3^2 & c_4^2 & b_1^2 & b_2^2 & b_3^2 & b_4^2 \\ 0 & 0 & 0 & 0 & 0 & 0 & 0 & 0 & -a_1 b_1 & -a_2 b_2 & -a_3 b_3 & -a_4 b_4 \\ 0 & 0 & 0 & 0 & -a_1 c_1 & -a_2 c_2 & -a_3 c_3 & -a_4 c_4 & 0 & 0 & 0 & 0 \\ c_1^2 & c_2^2 & c_3^2 & c_4^2 & 0 & 0 & 0 & 0 & a_1^2 & a_2^2 & a_3^2 & a_4^2 \\ -b_1 c_1 & -b_2 c_2 & -b_3 c_3 & -b_4 c_4 & 0 & 0 & 0 & 0 & 0 & 0 & 0 & 0 \\ b_1^2 & b_2^2 & b_3^2 & b_4^2 & a_1^2 & a_2^2 & a_3^2 & a_4^2 & 0 & 0 & 0 & 0 \end{bmatrix}, \tag{19}$$

$$\mathbf{X} = \begin{bmatrix} k_{x1} & k_{x2} & k_{x3} & k_{x4} & k_{y1} & k_{y2} & k_{y3} & k_{y4} & k_{z1} & k_{z2} & k_{z3} & k_{z4} \end{bmatrix}^{\mathrm{T}},$$

$$\mathbf{D} = \begin{bmatrix} m(2\pi f_{\mathrm{xo}})^2 & 0 & 0 & m(2\pi f_{\mathrm{yo}})^2 & 0 & 0 & m(2\pi f_{\mathrm{zo}})^2 & 0 & 0 & I_{xx}(2\pi f_{\mathrm{rxo}})^2 & 0 & 0 & I_{yy}(2\pi f_{\mathrm{ryo}})^2 & 0 & I_{zz}(2\pi f_{\mathrm{rzo}})^2 \end{bmatrix}^{\mathrm{T}}.$$

Table 2: Modal frequency and energy distribution of UCE in the original scheme.

Order		1	2	3	4	5	6
Modal frequency (Hz)		5.82	8.66	12.75	19.97	23.58	26.89
Energy distribution (%)	x	0.2	2.0	**82.8**	0.1	14.4	0.6
	y	**98.5**	0.6	0.5	0.0	0.2	0.1
	z	0.6	**81.1**	2.8	0.8	0.0	4.7
	r_x	0.2	2.3	0.3	10.1	7.7	**79.3**
	r_y	0.0	13.9	3.2	**55.6**	22.1	15.2
	r_z	0.4	0.1	10.3	33.4	**55.5**	0.2

Table 3: Modal frequency and energy distribution of UCE by FDM.

Order		1	2	3	4	5	6
Modal frequency (Hz)		6.23	8.66	11.09	17.02	20.87	26.86
Energy distribution (%)	x	0.0	3.8	91.0	2.2	2.9	0.1
	y	**97.9**	0.1	0.3	0.4	0.1	0.1
	z	1.1	**85.8**	4.5	0.0	1.0	4.6
	r_x	0.4	2.2	0.3	0.6	13.9	**82.7**
	r_y	0.0	7.0	1.1	2.4	**80.0**	12.5
	r_z	0.6	0.1	2.8	**94.3**	2.1	0.0

To obtain the least squares solution of $\min \quad g(\mathbf{X}) = \|\mathbf{CX} - \mathbf{D}\|$, the calculation is performed according to the generalized inverse matrix calculation method [19]. If a particular value in the received vector $\mathbf{X}$ is outside the constraint range $\mathbf{X}^L \le \mathbf{X} \le \mathbf{X}^U$, the value can be set to be equal to the constraint boundary value. Thus, the least-squares solution satisfying the constraint condition is obtained.

Table 4: Modal frequency and energy distribution of UCE by IDM.

Order		1	2	3	4	5	6
Modal frequency (Hz)		6.90	9.07	10.47	17.08	24.38	31.88
Energy distribution (%)	x	0.3	87.7	1.2	6.2	0.6	0.0
	y	**98.5**	0.2	1.0	0.1	0.1	0.1
	z	0.6	5.3	**92.2**	0.1	1.2	4.7
	r_x	0.2	0.1	2.3	0.1	13.8	**83.4**
	r_y	0.0	1.0	2.7	0.8	**83.6**	11.9
	r_z	0.3	5.7	0.6	**92.6**	0.7	0.0

Table 5: Sperling index of car body center before and after optimization.

Scheme	200 km/h		300 km/h	
	Vertical	Lateral	Vertical	Lateral
Original scheme	2.258	2.117	2.551	2.473
FDM	2.253	2.098	2.514	2.474
IDM	2.210	2.093	2.428	2.277

6.2. Inverse Decoupling Method (IDM). The inverse decoupling method (IDM) provides a numerical solution of the stiffness vector of the rubber element, which has the highest decoupling degree of UCE and the closest modal frequency to the optimized one. It is based on the boundary conditions of the rubber element stiffness satisfying the allowable range of production and installation. The mathematical model based on IDM can be reduced to the following equation:

$$\begin{aligned} \min \quad & g(\mathbf{X}) = \sum_{j=1}^{6} \alpha_j \left(1 - \max_{k=1,2,\ldots,6} \mathbf{EP}(k, j)\right)^2 + \sum_{j=1}^{6} \beta_j \left(\frac{f_j(\mathbf{X}) - f_{\mathrm{jo}}}{f_{\mathrm{jo}}}\right)^2, \\ s.t. \quad & \mathbf{X}^L \le \mathbf{X} \le \mathbf{X}^U, \\ & f_j^L \le f_j(\mathbf{X}) \le f_j^U, \quad j = 1, 2, \ldots, 6. \end{aligned} \tag{20}$$

In the above equation, the first term is the decoupling target. The smaller is its value, the higher decoupling degree is obtained. The second term is the modal frequency target. The smaller is the value, the closer are the modal frequencies to the optimum ones. Parameters α_j and β_j are weight coefficients, while f_j^L and f_j^U are the lower and upper limits of each mode frequency, respectively. Equation (19) is solved by the genetic algorithm, which applies to this case and has a strong ability of global optimization [20, 21].

7. Decoupling Optimization Calculation

7.1. Decoupling Degree Analysis. To demonstrate the decoupling optimization procedure, a test calculation of the original scheme is provided for UCE vertical natural frequency of 10.5 Hz, with the following coupling vibration working condition: a transverse eccentric distance of 0.60 m and an eccentric longitudinal distance of 0.75 m. The three-directional stiffness of the rubber component is designed via Eqs. 2–4. The six-order modal frequency and energy distribution of UCE are shown in Table 2. Here the second-order modal frequency is 8.66 Hz, which corresponds to the vibration mode with dominant bouncing vibration, which also couples with the pitch vibration. An apparent coupling is observed in the fourth-, fifth-, and sixth-order vibration modes. Combined with the engineering practice, according to the frequency configuration of UCE and the constraint conditions of the three-dimensional stiffness of the rubber elements via Equation (18)–(19), the three-dimensional stiffness of each rubber element is subjected to the decoupling optimization using FDM and IDM, respectively.

Tables 3 and 4 list the optimization results of the modal frequency and energy distribution of UCE when adopting FDM and IDM, respectively. It follows that the vibration

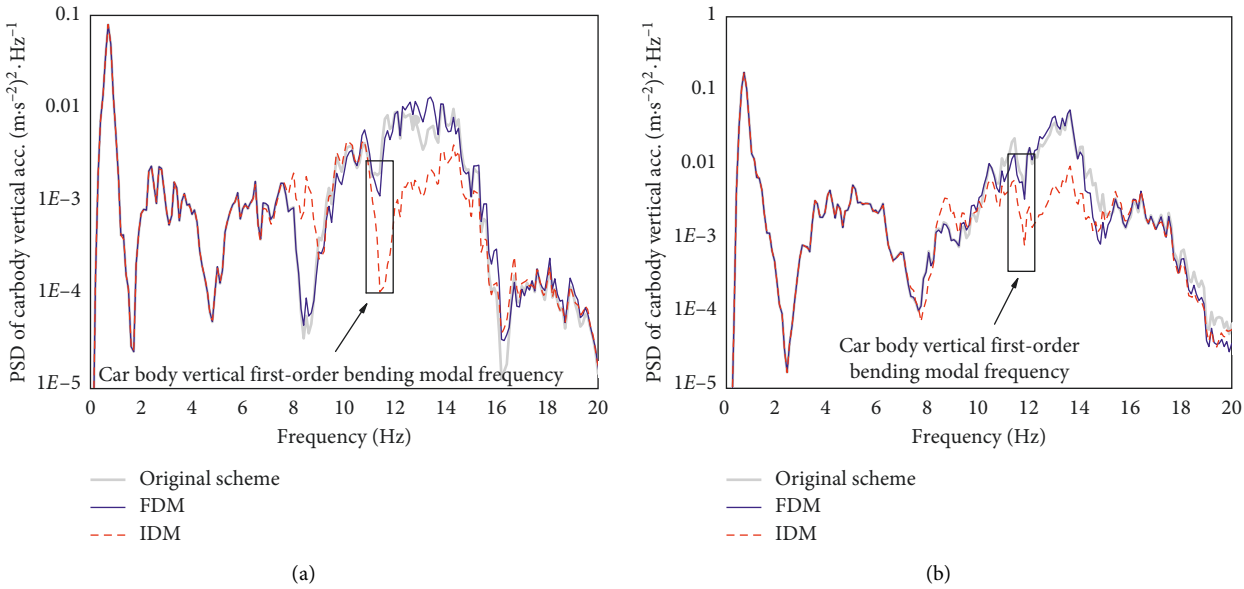

Figure 12: The power spectrum of car body vertical vibration acceleration. (a) The speed of 200 km/h. (b) The speed of 300 km/h.

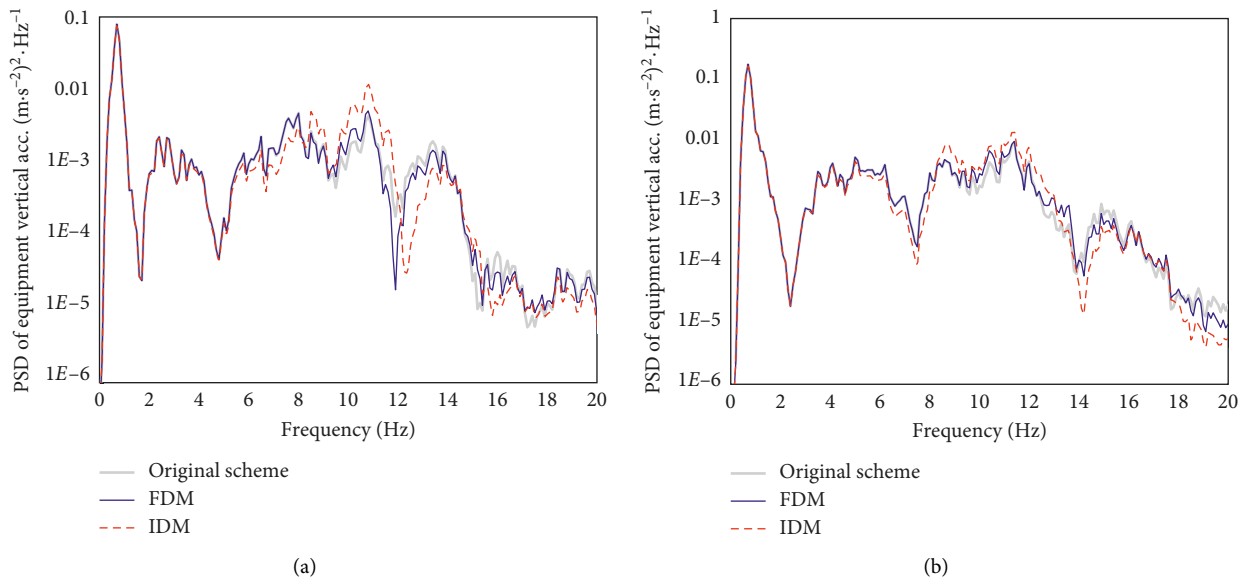

Figure 13: The power spectrum of UCE vertical vibration acceleration. (a) The speed of 200 km/h. (b) The speed of 300 km/h.

mode in each order has a favorable decoupling degree when adopting these two schemes. As compared to the original scheme, the second-order modal frequency through the FDM scheme (with dominant bouncing vibration) changes little, and the decoupling degree increases slightly. However, the decoupling degrees of the fourth-, fifth-, and sixth-order vibration modes increase. In the IDM scheme, the frequency of the vibration mode with the dominant bouncing vibration is 10.47 Hz, which is close to the design value. At the same time, the decoupling degrees of the fourth-, fifth-, and sixth-order vibration modes are also improved significantly.

Regarding the computational efficiency and accuracy, FDM can rapidly obtain the optimal values of the stiffness vector $\mathbf{X}$, the mode decoupling degree approaches 100%, and the mode frequency approaches the optimal frequency with no repeated iterations required. However, the internal elements of the vector $\mathbf{X}$ may be beyond the constraint range $\mathbf{X}^L \le \mathbf{X} \le \mathbf{X}^U$. Therefore, this method needs to be modified by an assignment method. As a result, the decoupling degree of some modes may be deteriorated, and there will also be a specific deviation between the modal and optimal frequencies. The IDM has high calculation accuracy; through a reasonable selection of control parameters, such as the crossover and mutation probabilities of the genetic algorithm, it achieves traversal solutions within the range of stiffness constraints $\mathbf{X}^L \le \mathbf{X} \le \mathbf{X}^U$. However, a large number of internal elements in the stiffness vector $\mathbf{X}$ require the algorithm to have a sufficient population and number of

iterations, in order to obtain good calculation accuracy. Therefore, IDM is less computationally efficient. In practical applications, the decoupling optimization method can be reasonably selected, according to the specific calculation efficiency and accuracy requirements.

7.2. Vibration Reduction Analysis. Table 5 shows the vertical Sperling index of the car body center when the above three schemes are applied in UCE. As compared to the original scheme, FDM has an unapparent influence of improvement on the ride quality. Both the vertical and lateral ride quality of the car body center is improved when IDM is applied. Moreover, the higher the running speed, the higher the reduction of the vehicle ride quality.

Figures 12 and 13 depict the power spectrum density of the vertical vibration acceleration of the car body center and UCE at speeds of 200 and 300 km/h, respectively. As seen in Figure 12, the car body vibration at the original vertical first-order bending frequency (11.60 Hz) will be suppressed when the vibration reduction design based on the dynamic vibration damping is applied in UCE. As compared to the original and FDM schemes, the suppression effect is more apparent when IDM is adopted. This can be attributed to the fact that IDM keeps the vertical vibration frequency near the optimal design frequency of 10.5 Hz while ensuring the favorable decoupling degree of the six-order vibration mode of UCE. As seen in Figure 13, the vertical vibration energy of UCE increases with a limited amplitude. This is because the damping of the rubber component consumes some energy during the vibration transfer. The above findings indicate that the UCE suspension system, whose decoupling degree was optimized and designed via the DVA theory, can achieve a better damping effect.

7. Conclusion

Based on the DVA theory, the vertical vibration natural frequency of UCE is assessed and optimized in this study. The influence of UCE coupling vibration on the DVA effect, as well as related mechanisms, are also investigated. The results obtained indicate that the eccentricity of UCE has a negative impact on the vehicle ride quality. This is attributed to the eccentricity inducing a coupling phenomenon between vibration in the six DOF directions of UCE. The vibration mode and frequency also change significantly. Thus, the natural frequency of UCE deviates from the designed initially optimal value, resulting in the deterioration of the damping effect and vehicle ride quality. Therefore, during the vibration reduction design of UCE for a high-speed EMU train, the coupling vibration of equipment should be carefully considered.

Two decoupling design optimization methods are proposed to make the vibrations in six DOF directions of UCE act individually at the optimal frequency. Collaborative optimization of the three-directional stiffness of rubber components in the suspension system of UCE is conducted with the decoupling degree and optimal frequency as the optimization objective and the rubber component's three-directional stiffness as the constraint condition. The calculation results imply that the decoupling degree of each order vibration mode of UCE is favorable. Also, the suspension system exhibits an apparent vibration reduction effect, and the vehicle ride quality is effectively improved.

Data Availability

The data used to support the findings of this study are available from the corresponding author upon request.

Conflicts of Interest

The authors declare that there is no conflicts of interest regarding the publication of this paper.

Acknowledgments

This work was supported by National Natural Science Foundation of China (grant no. 51805373) and the National Science and Technology Support Program project (grant no. 2015BAG19B02).

References

[1] D. Gong, J. Zhou, and W. Sun, "Influence of under-chassis-suspended equipment on high-speed EMU trains and the design of suspension parameters," *Proceedings of the Institution of Mechanical Engineers, Part F: Journal of Rail and Rapid Transit*, vol. 230, no. 8, pp. 1790–1802, 2016.

[2] J. Zhou, Z. Wei, W. Sun, and L. Ren, "Vibration reduction analysis of the dynamic vibration absorber on the flexible car body of railway vehicles," *China Railway Science*, vol. 30, no. 3, pp. 86–90, 2009.

[3] D. Gong, J. S. Zhou, and W. J. Sun, "On the resonant vibration of a flexible railway car body and its suppression with a dynamic vibration absorber," *Journal of Vibration and Control*, vol. 19, no. 5, pp. 649–657, 2013.

[4] M. Z. Ren, "A variant design of the dynamic vibration absorber," *Journal of Sound and Vibration*, vol. 245, no. 4, pp. 762–770, 2001.

[5] A. D. G. Silva, A. A. Cavalini Jr., and V. S. Steffen Jr., "Fuzzy robust design of dynamic vibration absorbers," *Shock and Vibration*, vol. 2016, no. 1, Article ID 2081518, 10 pages, 2016.

[6] Y. R. Wang and C. Y. Lo, "Design of hybrid dynamic balancer and vibration absorber," *Shock and Vibration*, vol. 2014, no. 5, Article ID 397584, 18 pages, 2014.

[7] F. Ma, A. Imam, and M. Morzfeld, "The decoupling of damped linear systems in oscillatory free vibration," *Journal of Sound and Vibration*, vol. 324, no. 1–2, pp. 408–428, 2009.

[8] T. Jeong and R. Singh, "Analytical methods of decoupling the automotive engine torque roll axis," *Journal of Sound and Vibration*, vol. 234, no. 1, pp. 85–114, 2000.

[9] Y. Suzuki and K. Akutsu, "Theoretical analysis of flexural vibration of car body," *QR of RTRI*, vol. 31, no. 1, pp. 42–48, 1990.

[10] D. Gong, J. S. Zhou, W. J. Sun, Y. Sun, and Z. Xia, "Method of multi-mode vibration control for the carbody of high-speed electric multiple unit trains," *Journal of Sound & Vibration*, no. 409, pp. 99–111, 2017.

[11] R. J. Guyan, "Reduction of stiffness and mass matrices," *AIAA Journal*, vol. 3, no. 2, pp. 1133–1145, 1965.

[12] P. F. Carlbom, "Combining MBS with FEM for rail vehicle dynamics analysis," *Multibody System Dynamics*, vol. 6, no. 3, pp. 291–300, 2001.

[13] A. Mirza, A. Frid, and J. C. O. Nielsen, *Reduction of Train Induced Ground Vibration by Vehicle Design. Noise and Vibration Mitigation for Rail Transportation Systems*, pp. 523–530, Springer Berlin Heidelberg, Berlin, Germany, 2015.

[14] D. Chen, Y. Ma, W. Sun, X. Guo, and X. Shi, "Research of design and vibration reduction of dual mass flywheel with arc helix spring," in *Proceedings of 2011 International Conference on Electronic and Mechanical Engineering and Information Technology (EMEIT)*, pp. 2706–2709, IEEE, Harbin, China, August 2011.

[15] K. Seto, "Control of vibration in civil structures," *Proceedings of the I MECH E Part I Journal of Systems and Control Engineering*, vol. 218, no. 1, pp. 515–525, 2004.

[16] F. T. Wang, J. S. Zhou, and L. H. Ren, "Analysis of track spectrum density for dynamic simulations of high-speed vehicles," *Journal of the China Railway Society*, vol. 24, no. 5, pp. 21–27, 2002.

[17] Y.-C. Cheng and C.-T. Hsu, "Running safety and comfort analysis of railway vehicles moving on curved tracks," *International Journal of Structural Stability and Dynamics*, vol. 14, no. 4, pp. 1272–1299, 2014.

[18] B. Sun, Q. Zhang, Q. Sun, Y. Li, M. Zhang, and S. Li, "Study on decoupled engine mounting system," *Journal of Vibration Engineering*, vol. 7, no. 3, pp. 240–245, 1994.

[19] A. B. Kucherov, "The method of inverse iterations for the calculation of the minimal and maximal eigenvalues of a cyclic tridiagonal matrix," *Numerical Methods of Linear Algebra*, pp. 103–111, 1982.

[20] J. H. Holland, *Adaptation in Natural and Artificial Systems: An Introductory Analysis with Applications to Biology, Control, and Artificial Intelligence*, Michigan Press, Ann Arbor, MI, USA, 1975.

[21] D. E. Goldberg, *Genetic Algorithms in Search, Optimization, and Machine Learning*, Addison- Wesley Pub. Co., Boston, MA, USA, 1989.